Photophysics of 1-Aminonaphthalene: A Theoretical and Time-Resolved Experimental Study

Raúl Montero, Asier Longarte, Álvaro Peralta Conde, Carolina Redondo, and Fernando Castaño*

Departamento de Química-Física, Facultad de Ciencia y Tecnología, Universidad del País Vasco, Apartado 644, ES-48080 Bilbao, Spain

Israel González-Ramírez, Angelo Giussani, Luis Serrano-Andrés, and Manuela Merchán*

Instituto de Ciencia Molecular, Universitat de València, Apartado 22085, ES-46071 Valencia, Spain

Received: June 23, 2009; Revised Manuscript Received: September 18, 2009

The photophysics of 1-aminonaphthalene (1-napthylamine, AMN) has been investigated on the basis of a constructive experimental−theoretical interplay derived from time-resolved measurements and high-level quantum-chemical ab initio CASPT2//CASSCF calculations. Transient ionization signals at femtosecond resolution were collected for AMN cold isolated molecules following excitation from the vibrationless ground level to a number of vibrational states (within the pump resolution) in the lowest accessible excited state and further multiphoton ionization probing at 500, 800, and 1300 nm. Theory predicts two $\pi\pi^*$ states, ^1L_b and ^1L_a, as the lowest singlet electronic excitations, with adiabatic transitions from S_0 at 3.50 and 3.69 eV, respectively. Since the associated oscillator strength for the lowest transition is exceedingly small, the ^1L_b state is not expected to become populated significantly and the ^1L_a state appears as the main protagonist of the AMN photophysics. Though calculations foresee a surface crossing between ^1L_a and the lower ^1L_b states, no dynamical signature of it is observed in the time-dependent measurements. In the relaxation of ^1L_a, the radiant emission competes with the intersystem crossing and internal conversion channels. The rates of these mechanisms have been determined at different excitation energies. The internal conversion is mediated by a $^1L_a/S_0$ conical intersection located 0.7 eV above the ^1L_a minimum. The relaxation of a higher-lying singlet excited state, observed above 40 000 cm^{-1} (4.96 eV) and calculated at 5.18 eV, has been also explored.

1. Introduction

Understanding the photophysical properties of simple aromatic chromophores, in particular, benzene and naphthalene derivatives, is the key stone to model many photoinduced phenomena in chemistry and biology, some of the most relevant ones being electronic energy transfer processes, photosynthesis, and photochemistry of DNA and RNA bases. In the case of monosubstituted naphthalenes, and despite of the enormous theoretical and experimental effort intended to relate their electronic structure to the observed photophysical behavior, many questions still remain open.

The electronic spectroscopy of naphthalene is dominated by two nearby $\pi\pi^*$ transitions involving two singlet states, labeled as ^1L_b (S_1) and ^1L_a (S_2) in Platt's nomenclature, with different orientation of the in-plane transition dipole moment, along the long and short molecular axes, respectively.[1] It is well-known that the oscillator strength of the lowest $S_1 \leftarrow S_0$ transition is low, gaining intensity via Herzberg−Teller coupling with the nearby ^1L_a state. The UV spectroscopy of naphthalene has been extensively studied[2−6] and used as a benchmark to develop nonadiabatic models for vibronically induced couplings.[7] Recently our group has investigated the nature of the nonadiabatic coupling between the ^1L_a and ^1L_b states of naphthalene.[8] The time-resolved study showed that the populated ^1L_a state internally converts to the lower ^1L_b state in 30 fs. This ultrafast dynamics points toward a coupling mechanism governed by a conical intersection connecting both states.

Substitution in the naphthalene ring by electron donor and/or acceptor groups may alter the relative energy and coupling between the S_1 and S_2 states, changing their properties and modifying the spectroscopic pattern. In this sense, 1-aminonaphthalene (1-naphtylamine, AMN) has attracted considerable attention because of the perturbation that the amino NH_2 electron-donating group induces on the electronic spectrum of the naphthalene molecule. The gas-phase fluorescence spectra of AMN reported by Berden et al.,[9] and in more detail by Jiang and Levy,[10] show an anomalous fluorescence pattern with sharp transitions superimposed to a red-shifted background. Moreover, a high-resolution study of the lowest vibronic feature observed in the fluorescence excitation spectrum carried out by Berden et al.[9] revealed a b-type transition which suggests a reversal of the ^1L_b and ^1L_a states ordering with respect to the naphthalene molecule. The exhaustive work performed by Rückert et al. on 1-aminonaphthalenes[11] highlighted the role of the amino group twist angle on the $^1L_a/^1L_b$ state coupling, bringing forward the influence of an internal conversion relaxation channel in the photophysical picture of the system.

The combination of time-resolved techniques in the femtosecond time scale applied to gas-phase isolated species with quantum-chemical ab initio calculations on excited states will be demonstrated here to be an extremely powerful approach to elucidate the wavepacket dynamics and/or the population flow

* To whom correspondence should be addressed. Phone: ++ 34 94 601 2533 (F.C.); ++ 34 96 354 31 55 (M.M.). Fax: ++ 34 94 464 85 00 (F.C.); ++ 34 94 464 85 00 (M.M.). E-mail: f.castano@ehu.es (F.C.); Manuela.Merchan@uv.es (M.M.).

10.1021/jp9058752 CCC: $40.75
Published on Web 10/21/2009

along the nonradiative relaxation pathways. The present study takes advantage of the interplay between theory and experiment to provide new insights on the photophysics of the AMN molecule. The following aspects of the problem have been investigated: the character of the absorbing and emitting states, the nature of the $^1L_a/^1L_b$ state coupling, and the involved decay pathways. We have carried out experiments on the system relaxation following excitation at a number of energies, from the first vibronic feature observed in the $S_1 \leftarrow S_0$ electronic spectrum at 332.8 nm (30 045 cm^{-1}, 3.73 eV) up to the $S_3 \leftarrow S_0$ transition at 235 nm (42 553 cm^{-1}, 5.28 eV). The employed transient ionization technique has proved to be very sensitive to the location of the wavepacket along the photo-excited state potential energy surface,[12] when the appropriate probe wavelength is chosen. Subsequently, a number of probe wavelengths in the 500−1550 nm range were tested. At all wavelengths the occurrence of resonant ionization, which would enhance the selectivity of the ionization process, was analyzed by collecting the polarization anisotropy decay.

From the theoretical viewpoint, the multiconfigurational perturbation quantum-chemical ab initio CASPT2//CASSCF method[13] has been employed to compute the low-lying electronic states of the AMN molecule. The use of such a well-established and general methodology in the calculation of excitation energies, oscillator strengths, transition dipole directions, together with accurate descriptions of the potential energy hypersurfaces (PEHs) by computing minimum energy paths (MEP), state minima, and conical intersection (CI) structures, leads to an accurate and predictive description of the photophysical parameters which has helped us to rationalize the experimental results.

The collected experimental and theoretical evidence support that excitation of AMN at the fundamental transition wavelength (30 045 cm^{-1}, 3.73 eV)[5,6] yields mostly the ^1L_a state. The $S_0 \rightarrow (S_2)\ ^1L_a$ adiabatic transition is computed to be slightly higher in energy than the almost forbidden $S_0 \rightarrow (S_1)\ ^1L_b$ transition. Although the computed MEP profile shows a crossing between the ^1L_a and ^1L_b states, no dynamical signature of it has been found in the time-dependent experimental measurements at any of the excitation energies. In this picture, the wavepacket would stay in the initially prepared ^1L_a surface after going through the crossing region. In addition to fluorescent emission, intersystem crossing (isc) and internal conversion (IC), the latter via a $^1L_a/S_0$ CI, participate in the quenching of the ^1L_a state. The rates of these competing processes are investigated in the range of the employed excitation energies. The appearance and ultrafast relaxation of a higher-lying singlet state at energies above 250 nm (40 000 cm^{-1}, 4.96 eV) is also explored.

2. Experimental and Theoretical Methods

The time-resolved experimental studies on AMN have been carried out in a mass spectrometer, using the transient ionization technique[14] with multiphoton probing. High-purity AMN (>98%) purchased from Aldrich was heated up to 80 °C and seeded in Ar. The mixture at a stagnation pressure of 1−2 atm was expanded through an electromagnetic valve (General Valve) and skimmed before entering the ionization region of the mass spectrometer. The formed ions were extracted and accelerated toward a dual 18 mm microchannel plate (MCP) detector placed at the end of the 80 cm linear time-of-flight tube.

The light pulses were generated with a Ti:sapphire oscillator-regenerative amplifier laser system which provides a 1 kHz train of 40 fs pulses at the fundamental wavelength (800 nm). The amplifier output was split in several beams used to pump two noncollinear optical parametric amplifiers (NOPAs) and a third harmonic generator. The produced wavelengths cover the range of 230−10000 nm and are utilized as pump or probe at convenience. In some experiments the 800 nm radiation was used to probe the molecules. Slightly focused pump and probe beams were introduced collinearly in the mass spectrometer. The pump beam power density was kept around 10^8 W/cm^2 and the probe in the $10^{11}-10^{13}$ W/cm^2 range. The beams were linearly polarized forming an angle of 54.7° between the polarization planes ("magic-angle" configuration), except for the anisotropy measurements. Pump−probe delays were varied with an optical delay line based on the continuous motion of a retroreflector with 150 ps total travel. The amplitude and period of the displacement was driven by a function generator, and the instantaneous position of the mirror was monitored and stored in a PC computer. For long time decays a second delay line based in a stepper motor and with a total travel of 1.3 ns was employed.

The masses spectrum was monitored in a digital oscilloscope. The intensities of a maximum of three masses versus the pump−probe delay were simultaneously registered for each valve shot with boxcar integrators (Stanford SR250). The integrated intensities were read by an A/D converter and stored in a PC computer for analysis. The maximum repetition rate used to register the ion signals was limited by the pumping capacity of the vacuum system and kept in the 100−200 Hz range. Typically 3×10^5 total valve shots were accumulated in one scan, for an average of 3×10^3 points at each delay time. The nonresonant ionization signal of ethylene $(1 + n')$ is acquired simultaneously with the signals of interest, to obtain the zero-delay time and the correlation function of the pump with the nth power of the probe. From the ethylene cross-correlation signal and knowing the order of the process (derived from a measurement of the ion intensity vs probe energy), we find a value between 100 and 130 fs (depending on the wavelength) and 50 fs, for the pump and the probe pulses width (fwhm), respectively.

In the fitting of the collected transients wavepacket coherence was ignored. Instead, a kinetic approach based on rate equations was employed.[15] The model describes the probing of the population flow from different locations reached consecutively along the relaxation pathway. These locations can be placed on the same or different potential energy surfaces.

The light-induced fluorescence (LIF) spectrum of the molecule was recorded in a separate chamber where a free jet is produced by a pulsed valve (General Valve), and the fluorescence is collected and focused on a photomultiplier with a telescope. As excitation source the doubled output of a dye laser (DCM + rhodamine 640) pumped by the second harmonic of a Nd:YAG was used.

Regarding the employed theoretical methods, optimizations of minima, transition states (TS), PEH crossings, and MEPs have been performed initially at the CASSCF level of theory. MEPs have been built as steepest descent paths in which each step requires the minimization of the energy on a hyperspherical cross section of the PEH centered on the initial geometry and characterized by a predefined radius.[16] At the computed geometries, CASPT2 calculations on several singlet states were carried out in order to include the necessary dynamic correlation effects. The protocol is usually named CASPT2//CASSCF and has proved its accuracy repeatedly.[13,17−23] In some cases, at the computed CASSCF crossings, CASPT2 explorations at close geometries were performed in order to find minimum energy CASPT2 crossing points (MECP), related to conical intersec-

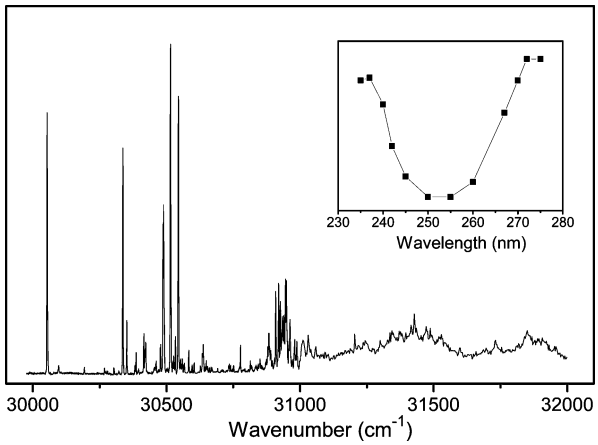

Figure 1. Fluorescence excitation spectrum of jet-cooled AMN. The inset shows the total ion signal intensity corrected (see text) as a function of the broad-band excitation wavelength.

tions, at the highest level of calculation.[24−26] The ANO-type one-electron atomic basis set ANO-S C,N[3s2p1d]/H[2s1p] was used throughout for energy optimizations and energy differences to obtain a balanced description of the PEHs. All calculations for the ground and $\pi\pi^*$-type states used a π active space of 12 electrons and 11 orbitals. An imaginary level-shift parameter of 0.1 au was employed to circumvent the presence of intruder states.[19] The standard zeroth-order CASPT2 Hamiltonian was used.[13] No symmetry restrictions were imposed during the calculations, which used in all cases the MOLCAS-6 set of programs.[27−29] From the calculated CASSCF transition dipole moments (TDM) and the CASPT2 band origin energies, the radiative lifetimes have been estimated by the Strickler−Berg relationship.[30,31]

3. Results

3.1. Experimental Results. Figure 1 shows the LIF spectrum of the AMN molecule seeded in a He supersonic expansion. The data were collected with the aim of covering a broader range than previous published measurements. In particular, the excitation was taken up to ∼600 cm^{-1} to the red of the 30 045 cm^{-1} band assigned to the ^1L_a state origin.[5,6] No additional bands or fluorescent emission was found; thus, this portion of the spectrum is not shown. The spectrum is in good agreement with that reported by Berden et al.,[9] Jiang and Levy,[10] and Lahmani et al.,[32] in similar conditions. Figure 1 inset depicts the excitation spectrum of the AMN molecule in the 280−230 nm region. The points represent the total one-color ionization signal (excitation intensity corrected) as a function of the excitation wavelength and were collected employing the output of a femtosecond OPA as excitation source. The measurement, similar to the gas-phase spectrum reported elsewhere,[33] is composed of two electronic transitions. The $S_1/S_2 \leftarrow S_0$ absorption appears below 260 nm, whereas the $S_3 \leftarrow S_0$ transition extends from there to higher energies. Despite the measurements were normalized to the excitation beam energy, the relative intensity of the transitions is affected by the lower transmission of the optics at shorter wavelengths.

The time evolution of the 1-aminonaphthalene ion signal (AMN^+) was recorded following excitation in the 330−235 nm range. The probing was carried out at 500, 800, and 1300 nm, looking for the higher sensitivity to the wavepacket dynamics. No species other than the parent ion and the AMN−28^+ uma fragment was observed in the mass spectrum. The temporal profile of this fragment signal (not shown) matches that of the parent ion, revealing that its formation takes place in the ion after the absorption of probe photons.[34]

Figure 2 collects the short time scale transients recorded in the AMN^+ mass channel, exciting at the indicated energies in the $^1L_a/^1L_b \leftarrow S_0$ transition range and probing with 500 nm (two photons), 800 nm (three photons), and 1300 nm (four photons) light pulses. Exciting at 267 nm and probing with 1300 nm yields a signal too weak to obtain an acceptable transient. Additionally, two measurements were collected with the probe at 1550 nm (five photons). That with the excitation at 298 nm shows a peak at $t = 0$ attributed to nonresonant ionization ($1 + 5'$) signal, probably enhanced by the accidental resonance with the S_n electronic state at ∼48 000 cm^{-1} ($1 + 2'$).

The most remarkable feature in these transients is the absence of dynamics attributed to $^1L_a/^1L_b$ state coupling (τ_1). The only time constant computed (apart from the $\tau = \infty$ used to fit the signal background) is a fast τ_0 with a value between 0 and 10 fs, derived from the fit of the raising portion of the transients collected with the 500 nm probe. This time constant may be assigned to wavepacket motion out of the Franck−Condon (FC) region, but it may also be caused by an eventual nonresonant ionization contribution ($\tau_0 = 0$). Ionization with the 500 nm probe occurs resonantly through an electronic excited state, making the probing particularly sensitive to the wavepacket dynamics. This aspect is further confirmed by the polarization anisotropy measurements shown in Figure 3. The nonzero value of the anisotropy function measured at the indicated excitation wavelengths reveals that the probe meets a resonance in the ionization process. Two distinct time-dependent processes are observable in the anisotropy decays. In the short time range (Figure 3a), a component between 0 and 10 fs (τ_0) matches that observed in the magic-angle transients. The long-range decays (Figure 3b) are assigned to rotational dephasing and have been simulated by expressions that describe the macroscopic anisotropy signal as a function of the rotational states Boltzmann distribution (see ref 35, eq 35). From the fittings of the different excitation energies, a rotational temperature between 10 and 15 K has been computed.

The relaxation of AMN was also investigated on longer time scales yielding a lifetime (τ_2) that shortens with the excitation energy, from 0.94 ns at 311 nm to 13.7 ps at 235 nm. The transients recorded at all the excitation energies with the 800 nm probe are shown in Figure 4a, and the extracted τ_2 values are summarized in Table 1. In addition, long time scale transients were recorded probing with 500 nm pulses (Figure 4b), which in contrast with those probed with the 800 nm light, do not show a constant offset. This background is attributed to the population of a long-living triplet state that does not ionize when the 500 nm probe is used. The presence of an isc relaxation channel was previously proposed.[10] Therefore, the τ_2 component should account at low excitation energies for the sum of the isc and IC rates, having similar contributions from both mechanisms. The IC is mediated by a $^1L_a/S_0$ CI predicted by our calculations, and its rate increases as the excitation energies approaches the surface crossing (see discussion below).

The relaxation of AMN was also studied following excitation to the higher-lying excited state observed in the ionization excitation spectrum of Figure 1 inset. Figure 5 shows the transient recorded with 235 nm pump and 800 nm probe together with the ethylene nonresonant ionization signal. The time-dependent signal exhibits in the short time scale a 80 ± 10 fs component, followed by a much longer one of 14 ± 2 ps. The former is attributed to ultrafast $S_3/^1L_a$ relaxation presumably

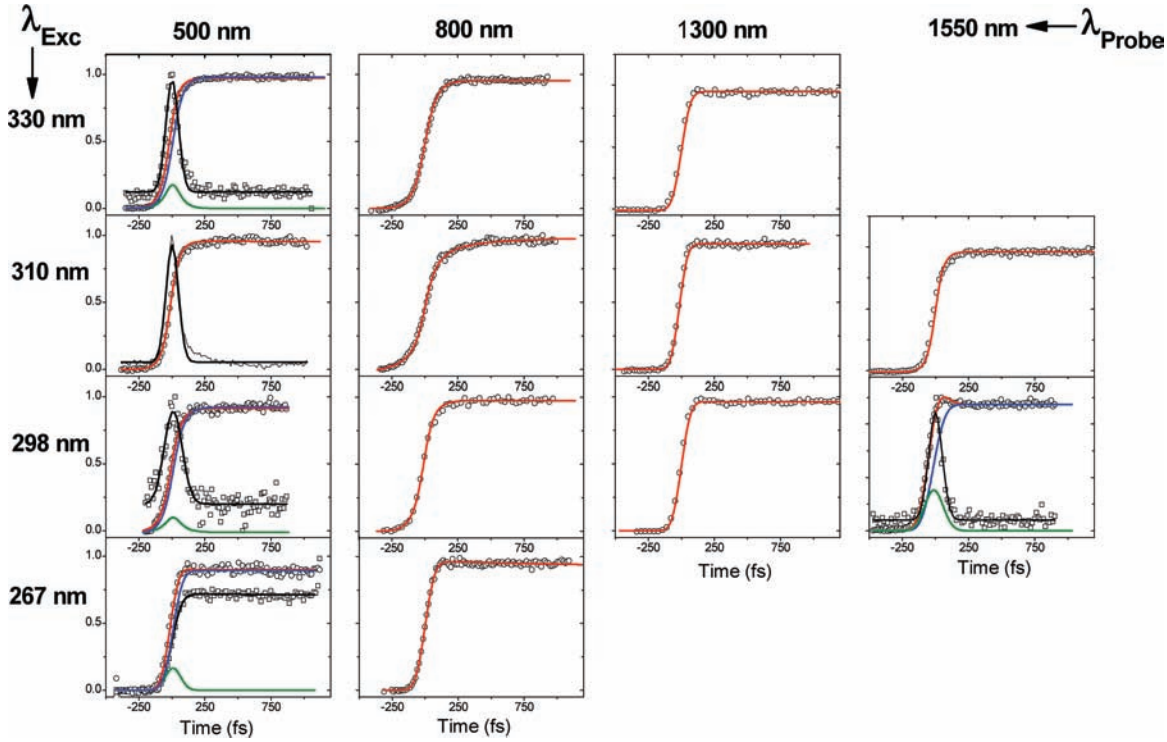

Figure 2. Short-range decays of AMN collected at the indicated pump (rows) and probe (columns) wavelengths. Experimental data are shown as circles and decay fits by lines. In those cases where more than a $\tau = \infty$ constant was required in the fitting, the individual components are plotted (see text). The nonresonant ionization signal of ethylene is shown for comparison except for the 267 nm excitation wavelength. In this case, due to the weak ethylene signal obtained, aniline resonant ionization through a nanoseconds lifetime intermediate state was employed to determine $t = 0$.

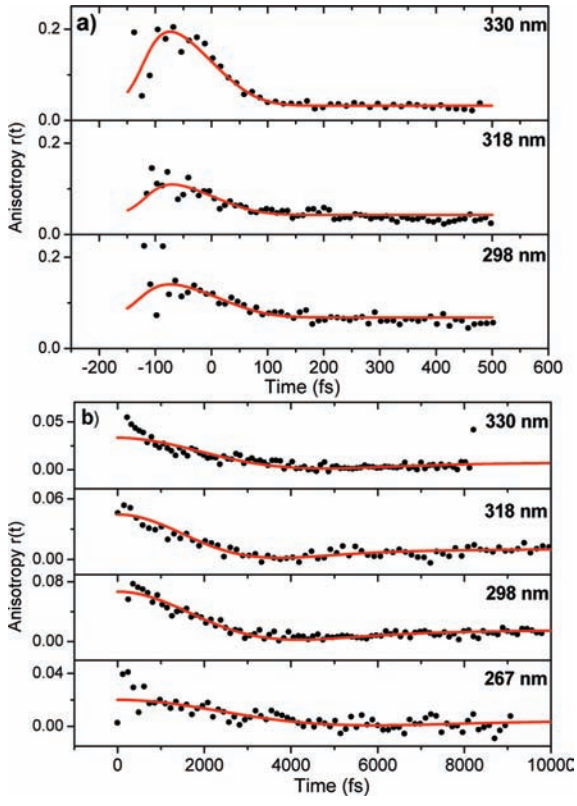

Figure 3. Short-range (a) and long-range (b) polarization anisotropy decays of AMN collected by exciting at the indicated wavelengths and probing at 500 nm. The low signal at 267 nm precluded the collection of a short-range transient. Experimental data are shown as circles and decay fits by lines.

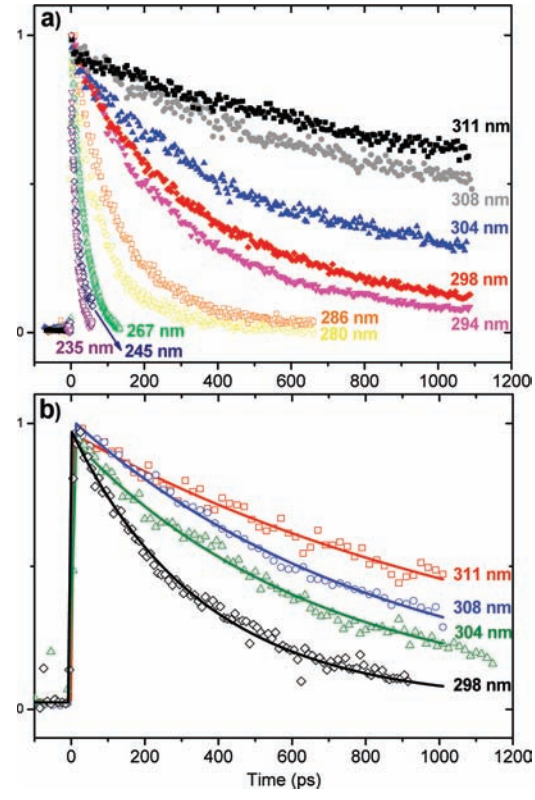

Figure 4. (a) AMN long-range decays recorded by exciting at the indicated wavelengths and probing with 800 (a) and 500 nm (b) wavelengths. For the former only the experimental data are shown, whereas for the latter the exponential fittings are also included. The time constants extracted for both probe wavelengths are collected in Table 1.

TABLE 1: Lifetimes Extracted from the Fittings of the Long-Range AMN Transients Shown in Figure 4[a]

	τ_2 (ps)	
excitation (nm)	probe 800 nm	probe 500 nm
311	940 ± 138	1300 ± 200
308	710 ± 100	772 ± 105
304	513 ± 70	657 ± 60
298	348 ± 30	365 ± 25
294	290 ± 35	
286	120 ± 10	
280	84 ± 6	
267	35 ± 5	
245	16 ± 2	
235	14 ± 2	

[a] The τ_2 constants are the sum of internal conversion and intersystem crossing lifetimes (see text for details).

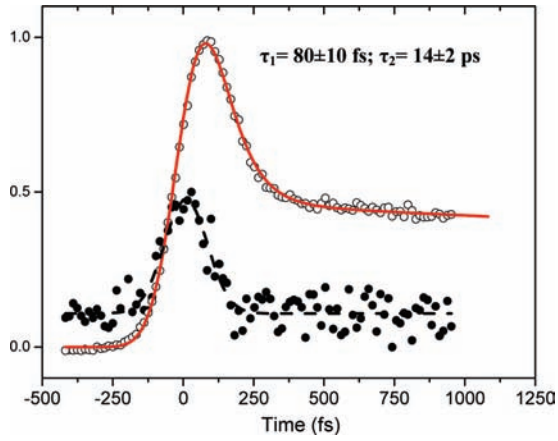

Figure 5. Short time scale transient of AMN collected with 235 nm excitation and 800 nm probe wavelengths. The dashed line corresponds to the 1 + 4′ nonresonant ionization signal of ethylene. Experimental data are shown as circles and decay fittings by lines.

induced by a CI intersection, whereas the latter corresponds to the above-mentioned τ_2 $^1L_a/S_0$ internal conversion.

3.2. Theoretical Results. Tables 2 and 3 and Figures 6 and 7 summarize the most relevant theoretical results of the low-lying singlet and triplet electronic states of AMN computed by CASSCF and CASPT2 methodologies. Two singlet and two triplet excited states (labeled L_a and L_b in Platt's nomenclature) with $\pi\pi^*$ nature have been found as the low-lying excited electronic states, that is, those having photophysical relevance in the excitation region studied. As discussed later, states of pure $n\pi^*$-type character (involving the nitrogen lone-pair electrons) are found energetically too high, although charge transfer from the amino group toward the rings will be shown to play an important role. Tables 2 and 3 contain results for computed vertical absorptions, band origins, and vertical emission for the different states, together with other properties such as transition oscillator strengths, dipole moments, transition dipole moment directions, and radiative lifetimes. Those results are complemented with values on the relative position of the states and the transition dipole moments orientation, Θ_{TDM}, at the singlet states minima. Together with these properties, Figure 6 displays a MEP computed at the CASPT2//CASSCF level on the ^1L_a hypersurface starting at the FC ground-state optimized geometry, which freely leads to the ^1L_a minimum in a barrierless pathway. Along the relaxation process a crossing between the ^1L_a and the ^1L_b states takes place, the latter becoming the lowest in energy. Such crossing can be related with the presence of a conical intersection $(^1L_a/^1L_b)_{CI}$, which may, in principle, control the population transfer occurring along the state switch. As discussed below, the theoretical results are complemented with the calculation of the $(L_a/S_0)_{CI}$ CI, obtained as the MEPs between the two PEHs. Figure 7 displays the structures of the singular points optimized in the present work.

4. Discussion

Several theoretical predictions and experimental evidences point to ^1L_a as the state populated upon excitation in the range of the employed energies, 330−267 nm. First, calculations of Table 2 predict a substantially higher oscillator strength for ^1L_a than for ^1L_b. Second, the transition at 333.8 nm (3.71 eV) of the jet-cooled spectrum has been unambiguously assigned as the $^1L_a \leftarrow S_0$ band origin, having short-axis (*b*) polarization with a Θ_{TDM} angle of 72°,[9] in perfect accordance with our computed value at the ^1L_a state minimum, 73°. In addition, individual vibronic features of the fluorescent excitation spectrum (Figure 1) show lifetimes compatible with the allowed $^1L_a \leftarrow S_0$ transition.[32] Therefore, the remaining question is whether it is possible or not to excite the ^1L_b state from S_0 and what is the spectroscopic signature of this state. Although substitution on naphthalene position 1 by NH_2 was thought to cause a state order reversal.[9,10,36−38] our results compiled in Tables 2 and 3 clearly indicate that the ^1L_b band origin should lie below that of ^1L_a in AMN (3.50 and 3.69 eV, respectively). Since no other spectroscopic feature was found to the red of the ^1L_a state origin, we believe that, although probably the vibrationless ^1L_b transition is too weak to be observable, some vibronic features of this state may gain intensity from Herzberg−Teller coupling with ^1L_a and appear mixed in the latter state spectrum. A similar situation has been found recently for the $^1L_a/^1L_b$ state mixing in tryptamine.[39] Therefore, below the $^1L_a/^1L_b$ CI calculated to be 0.08 eV over the L_a surface minimum, the spectrum would be composed mainly of $^1L_a \leftarrow S_0$ vibronic bands. Some weak absorption lines of the ^1L_b state owing their intensity to Herzberg−Teller coupling with the ^1L_a state could also appear in this region. About 800 cm^{-1} to the blue of the $^1L_a \leftarrow S_0$ band origin, where the calculations predict the CI to be, the spectrum starts to show symptoms of congestion, reflecting the stronger mixing of both states.

At the ground-state optimized FC geometry the molecule has been shown to be almost planar, with pyramidalized and partial twist of the NH_2 group and out-of-plane dihedral angles of 49.9° and 10.2° (with respect to carbon in cis) for the hydrogen atoms 1a and 1b (cf. Figure 7), respectively. The nonequivalence of the amino hydrogen atoms, known as *peri effect*, is caused by a difference in the steric interactions with the adjacent hydrogen atoms of the naphthalene ring.[9] Relaxing the populated ^1L_a state along the computed MEP leads to a crossing between the PEHs of the ^1L_a and ^1L_b states, in which they exchange order, finally reaching the ^1L_a state minima. Such structure belongs to the S_1 PEH and has a totally planar conformation, with a shortened (0.074 Å) C−N bond length and changed bond alternation in the rings respect to the ground-state minimum, in agreement with the experimental results.[9] Therefore, those deformations will be correlated with the modes responsible for the evolution along the lowest-energy path. The PEH crossing found along the ^1L_a state relaxation path may be related here to the presence of a conical intersection $(^1L_a/^1L_b)_{CI}$ connecting both states. Calculations at the CASPT2 level predict this surface crossing to be at 3.77 (30 405 cm^{-1}), 0.27, and 0.08 eV above the ^1L_b and ^1L_a states origin bands, respectively. The ^1L_b state is known as a locally excited (LE) state and has an optimized structure similar to the ground state and also a twisted and pyramidalized

TABLE 2: Computed Spectroscopic Properties of the Low-Lying Singlet Excited States of 1-Aminonaphthalene (AMN)[a]

	vertical absorption/eV		band origin/eV		vertical emission/eV				
state	CAS	PT2 (*f*)[a]	CAS	PT2	CAS	PT2	μ/D[b]	Θ_{TDM}[c]	τ_{rad}/ns[d]
$^1(\pi\pi^*)$-L_b	4.15	3.80 (0.0008)[e]	3.86	3.50	3.66	3.44	1.36	−15	2754
$^1(\pi\pi^*)$-L_a	5.78	4.35 (0.0481)[e]	4.95	3.69[f]	4.27	3.20[g]	4.59	77	64[h]
$^3(\pi\pi^*)$-L_a	2.92	2.83	2.47	2.35	2.06	2.09	1.33		0.1 ms
$^3(\pi\pi^*)$-L_b	4.19	3.63					1.43		

[a] CAS, CASSCF level; PT2, CASPT2 level. Oscillator strengths within parentheses. [b] CASSCF dipole moment at the FC geometry. Ground-state μ is computed to be 1.20 D. [c] Transition dipole moment orientation (Θ_{TDM}), in degrees, referred to the inertial long axis (*a*) of the molecule, computed here at the S_0 optimized FC geometry. For definition see ref 9. [d] Calculated radiative lifetime (Strickler−Berg relationship, see text). [e] Experimental data (magnetic circular dichroism): band maxima, 3.90 and 4.17 eV (gap 2200 cm^{-1}), in hexane (ref 3). [f] Laser-induced fluorescence (LIF) in a supersonic jet. Band origin (T_0): 3.73 eV (30 045 cm^{-1}), short-axis polarized (refs 9 and 10). The computed result corresponds to T_e (ZPE has not been included). The presence of an overlapping second absorption band with long-axis polarized components (L_b) is suggested (ref 10). [g] Fluorescence band maximum: 3.31, 2.93, and 2.73 eV in cyclohexane, acetonitrile, and water, respectively (refs 3 and 4). [h] Estimated radiative lifetime: 13 ns (cyclohexane), 25 ns (butan-1-ol), and 43 ns (water) (ref 4).

TABLE 3: CASPT2 Relative Energies (ΔE/eV) at the Different Stationary Points of the Hypersurfaces Referred to the Ground State Computed at the Equilibrium Geometry, Dipole Moments, and CASSCF Computed Transition Dipole Moment Directions (Θ_{TDM}/deg)[a]

	$(S_0)_{min}$			$(S_1-L_b)_{min}$			$(S_1-L_a)_{min}$		
state	ΔE/eV	μ/D	Θ_{TDM}	ΔE/eV	μ/D	Θ_{TDM}	ΔE/eV	μ/D	Θ_{TDM}
S_0	0.00	1.20		0.06	1.21		0.49	1.48	
$^1(\pi\pi^*)$-L_b	3.80	1.36	−15	3.50 (T_e)	1.29	28	3.92	1.52	−1
$^1(\pi\pi^*)$-L_a	4.35	4.59	77	3.92	4.59	−84	3.69(T_e)	5.54	73[b]
$^3(\pi\pi^*)$-L_a	2.83	1.33		2.54	1.33		2.51	1.72	
$^3(\pi\pi^*)$-L_b	3.63	1.43		3.40	1.40		3.88	1.82	

[a] Θ_{TDM} referred as positive toward the amino group from the inertial long axis (*a*) of the molecule (ref 9). [b] Transition dipole moment orientation (Θ_{TDM}) of the T_0 band of AMN in a supersonic jet: 72°, short (*b*) axis polarized, that is, L_a type (ref 9).

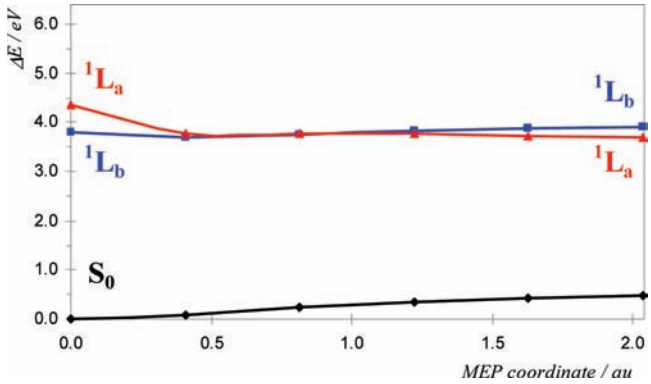

Figure 6. Computed CASPT2//CASSCF MEP along the hypersurface starting at the FC geometry (S_0 minimum) and freely leading to the ^1L_a state minimum. A crossing between ^1L_a and ^1L_b hypersurfaces is observable.

amino group with dihedral angles of 39.9 and 8.8°. Regarding the dipole moments of the ^1L_b and ^1L_a states, they are computed to be 1.36 and 4.59 D, respectively. The latter is 3.8 times that of the ground state (1.20 D), confirming the partial charge-transfer character of the ^1L_a state. Figure 8 displays a scheme of the photophysics of AMN based on our theoretical findings.

Time-dependent measurements after excitation in the 330−267 nm range (Figure 2) were performed aiming to gain information on the $^1L_a/^1L_b$ coupling predicted by the calculations. The only time constant extracted from those measurements is $\tau_0 = 0-10$ fs, as previously stated. This constant appears in the transients collected in the whole interval of excitation energies. Below ~31 000 cm^{-1} (322.6 nm), the spectral width of the individual vibronic features observed in the LIF excitation spectrum is not compatible with lifetimes shorter than 2 ps, precluding the assignation of τ_0 to an electronic dephasing event. Therefore, τ_0 could have two alternative origins: motion of the wavepacket out of the FC region favored by a resonance met in the absorption of the probe or a nonresonant ionization contribution.

A key question requiring further discussion is the absence of the predicted $^1L_a/^1L_b$ coupling signature from the recorded decays. Taking the theoretical calculations as a benchmark, several scenarios could be invoked to explain this fact: (i) An obvious interpretation is the insensitivity of the experiment to the $^1L_a/^1L_b$ surface crossing dynamics. Numerous examples can be found in the literature supporting the ability of the transient ionization technique to reflect the conversion of electronic to vibrational energy. Recently we have applied it to effectively disentangle the $^1L_a/^1L_b$ coupling in naphthalene.[8] AMN represents a more complicated situation due to the small energy gap predicted between the band origins of the involved electronic states, merely 1532 cm^{-1} (cf. Tables 2 and 3). However, the use of a resonant probe and anisotropy measurements aid to overcome this difficulty. It is unlikely that in the event of a $^1L_a/^1L_b$ surface crossing the transition probability to the resonant intermediate state remains constant. Furthermore, the anisotropy decays should reflect the change in the transition dipole moment associated to an eventual surface hoping, as observed in naphthalene.[8] (ii) An alternative explanation could be that the excitation populates both states with a ratio close to that the system will reach at the CI branching. Although, in principle, the ^1L_a has much higher oscillator strength, some ^1L_b vibronic transitions can gain intensity through Herzberg−Teller coupling, as pointed above. (iii) Finally, the absence of surface crossing signs can also be attributed to the properties of the wavepacket dynamics at the CI. The branching ratio, determined along the coupling coordinate by the wavepacket momentum and the PEH slopes, could favor that the system stays mainly on the initially prepared ^1L_a surface. Calculations able to model the CI topology are required in order to elucidate the plausibility of this scenario.

The slow component τ_2 observed in the time evolution of the AMN ion is attributed to the system relaxation to the ground-

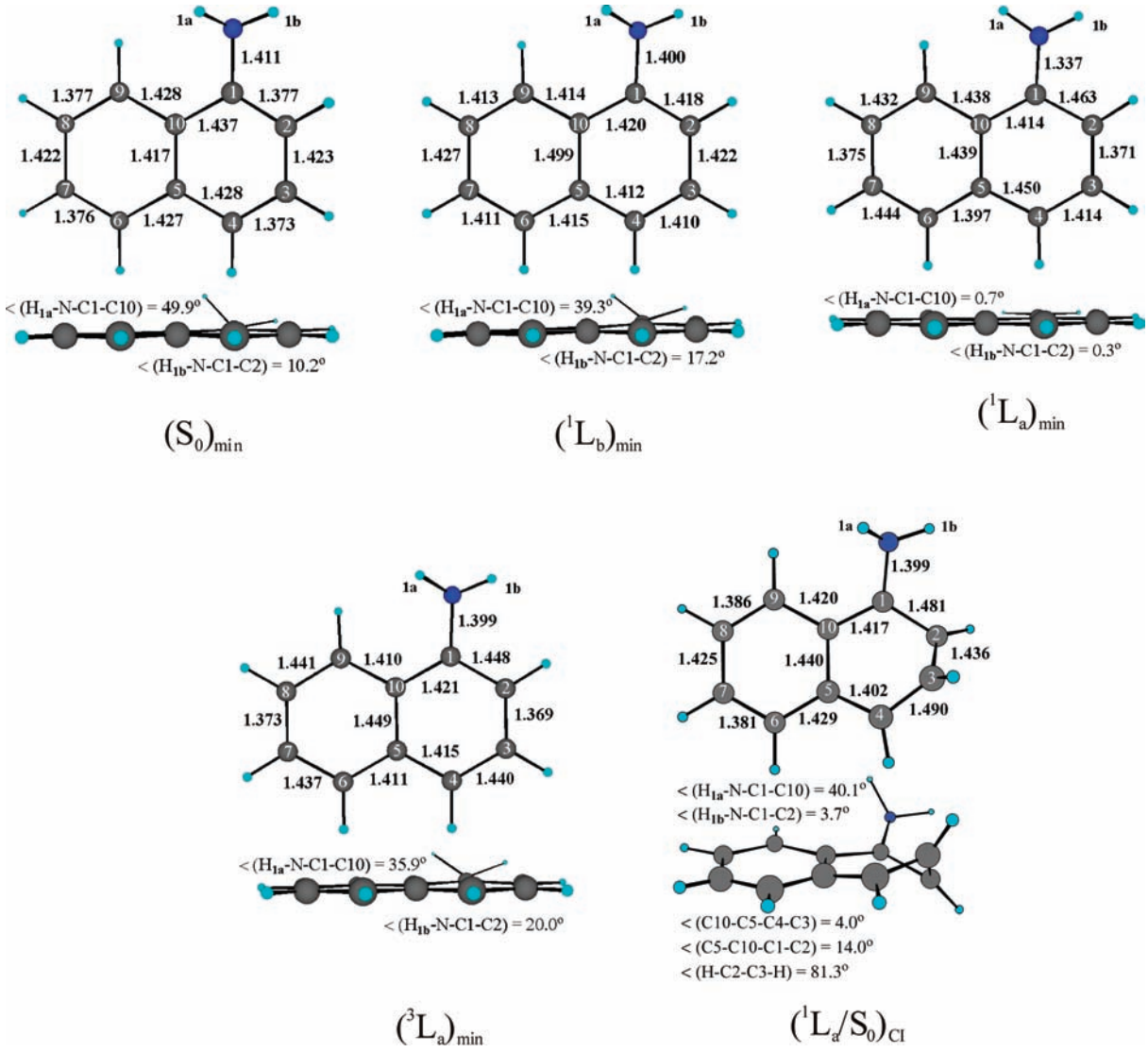

Figure 7. Main geometrical parameters of several optimized structures of AMN.

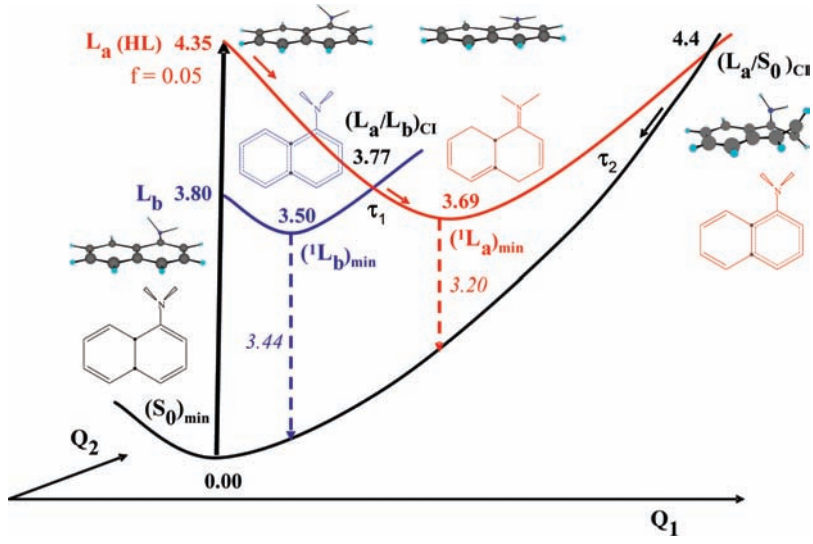

Figure 8. AMN photophysics scheme based on the theoretical and experimental results presented in the work. Energies are given in electronvolts with respect to the ground-state minimum.

state trough the $(^1L_a/S_0)_{CI}$ CI, mixed at low excitation energies with an isc process. As mentioned above, probing with 500 nm light (Figure 4b) does not ionize the triplet state, and thus, the constant background observed in the transients of Figure 4a disappears. Assuming an equal ionization probability at 800 nm for the initially populated singlet ^1L_a state and the triplet state,

we can relate in our kinetic model the offset to the observed time constant and then separate the contributions of IC and isc to τ_2. These results are collected in Table 1. The lifetimes are in accord with those reported by Rückert et al. for AMN in *n*-hexane.[11] The data of Table 1 show a significant increment in the IC rate with the excitation energy from 0.85 ns at 311 nm (3.99 eV) to 14 ps at 235 nm (5.28 eV). The steep raise is interpreted as the opening of the relaxation channel through the $^1L_a/S_0$ intersection when the excitation energy is enough to overcome the barrier toward $(^1L_a/S_0)_{CI}$, leading to an enhanced IC that competes with the ^1L_a fluorescent emission. The CASPT2 calculations place this intersection 0.7 eV over the ^1L_a state minimum and 4.4 eV over S_0. According to its structure, this crossing is characterized as a typical ethene-like CI,[40−42] in which a twisting of the C=C double bond leads to an out-of-plane deformation placing one hydrogen above and other below the plane of the ring (cf. Figure 7) forming a dihedral angle of 81.3° combined with a slight pyramidalization of the amino group.

The existence of the internal conversion pathway related to a $(^1L_a/S_0)_{CI}$ CI was advanced by Rückert et al.[11] from the study of 1-aminonaphthalenes radiative rates in solution. They determined for AMN in *n*-hexane an IC activation energy of 38 ± 8 kJ/mol (3176 cm^{-1}, 0.39 eV). Although our experimental measurements do not seem to anticipate a clear barrier, the CASPT2 calculations yield an upper bound of 0.7 eV for the crossing of the two surfaces in the isolated AMN with respect to the initially populated ^1L_a minimum. A full CASPT2 optimization of the CI would probably decrease the energy required to reach the PEH crossing closer to the experimental estimations.

The relaxation of AMN was also investigated following excitation to a higher-lying singlet state at 235 nm (5.28 eV). Two states are computed higher than ^1L_b and ^1L_a at the FC geometry, namely, S_3 and S_4, with 4.98 and 5.18 eV energies, 1.79 and 2.28 D dipole moments, and 0.0052 and 0.0528 $S_0 \leftarrow S_{3,4}$ oscillator strengths, respectively. The higher oscillator strength of S_4 permits us to assign it as the responsible of the absorption at 235 nm observed in the inset of Figure 1. The transients recorded following excitation of this band (Figure 5) show a biexponential behavior with the components: $\tau_1 = 80 \pm 10$ fs and $\tau_2 = 14 \pm 2$ ps. The electronic relaxation pathway is understood in a sequential way, where the prepared S_4 state relaxes to the lower $S_3/^1L_a/^1L_b$ manifold (mediated by CIs), proceeding from there to the ground state through the calculated $(^1L_a/S_0)_{CI}$.

On the light of the experimental and theoretical results presented, we may try to interpret previous results on the photophysics of AMN. The lack of experimental evidence of the $^1L_a/^1L_b$ surface crossing does not allow us to validate the dual-fluorescence model proposed for AMN.[10] Within this model, the red-shifted emission observed in addition to the sharp features when the zero-point level is excited is interpreted as the emission of a charge-transfer character state (^1L_a in this case) different from the locally excited ^1L_b. In our picture, ^1L_a would be the initially prepared state and the broad red-shifted emission a consequence of its geometry change with respect to the ground state.

Concerning the photophysics of the system in solvated environments, the increase of solvent polarity is related with the raise of fluorescence quantum yields (θ_f) and lifetimes (τ_f): $\theta_f = 0.47$, $\tau_f = 6.63$ ns (hexane), $\theta_f = 0.66$, $\tau_f = 12.4$ ns (diethyl ether), and $\theta_f = 0.86$, $\tau_f = 18.3$ ns (acetonitrile) and a decrease of the IC quantum yields from 0.13 (hexane) to 0.04 (acetonitrile).[11] This behavior was previously explained by the reduction of the S_2-S_1 gap in nonpolar solvents that rules the vibronic coupling between the excited states.[11] A stronger coupling between both states was then expected to favor the decay to the ground state, decreasing in that case the barrier for the IC from the S_1 to the S_0 state. As we recently emphasized,[24] the use of the energy gap between excited states as a measure of the strength of the vibronic coupling controlling the efficiency of the IC to the ground state may not be a valid argument related to the classical and frequently used Lim's proximity effect model.[24,43] The model is not applicable in many cases, and AMN is a good example of its failure. In fact, its initial hypothesis is erroneous. Contrary to previous proposals, which suspected a state reversal with respect to naphthalene,[11] the highly polar ^1L_a state is S_2 at the FC geometry, and as shown in Table 3, in polar solvents a large stabilization of the ^1L_a (S_2) state with respect to the ^1L_b (S_1) and the ground state can then be expected, diminishing the S_2-S_1 and S_2-S_0 energy gap and, thus, invalidating the initial hypothesis and the model. The analysis of the dipole moments of the states compiled in Table 3 provides an insight of the expected trends in polar media. For the ground and the ^1L_b states similarly low dipole moments have been computed at the FC geometry, 1.20 and 1.36 D, respectively, close to the experimental determination for the ground state, 1.55 D.[11] On the contrary, the ^1L_a state dipole moment is computed to be 4.57 D, a somehow small value if compared with the 7.2 D estimated using Onsager's solvatochromic shift procedure,[11] although this is a strategy with limited accuracy that tends to overestimate the excited-state dipole moments.[44,45] In any case the partial charge-transfer character of the ^1L_a state is confirmed. Figure 9 displays a density difference plot between the ground and the exited ^1L_a state at the ^1L_a minimum structure, in which the charge-transfer character of the excited state is enhanced. Excitation to the ^1L_a state is accompanied by a shift of the amino nitrogen and the substituted benzene charge toward the neighbor ring, resulting in a large, mainly long-axis polarized, dipole moment. The corresponding charge transfer is largely favored by the coplanarity of the amino group.

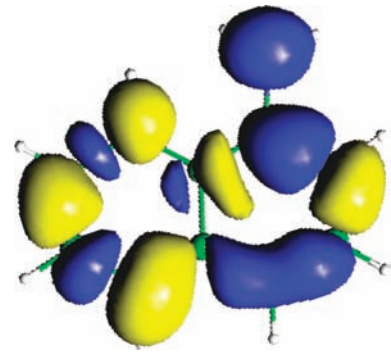

Figure 9. Density difference plot of the ^1L_a state of AMN with respect to the ground state at the ^1L_a minimum structure (isovalue 0.001). In the excitation the charge leaves the blue (dark) zones toward the yellow (light) areas, explaining the short-axis polarization of the corresponding transition, the long-axis polarized and large dipole moment of the excited state, and its partial charge-transfer character (from the amino group to the rings).

The alternative model we highlight here points out that the efficiency of any IC is related to the location and properties of the nearby conical intersection—$(^1L_a/S_0)_{CI}$—and with the barriers required to access the seam of the CIs, and neither to the gaps between higher excited states, S_1-S_2 ($^1L_b-^1L_a$), nor the location of the corresponding CI, $(^1L_b/^1L_a)_{CI}$, or the vibronic coupling between these two states. As a matter of fact, the S_2 state lies

in AMN higher than 2 eV at the $(^1L_a/S_0)_{CI}$ structure, and it can hardly have any influence in the position or shape of the CI. Therefore, we may state that the IC process related to the nanosecond-range lifetime of AMN in solvated phases is modulated only by the location and the barrier to access the $(^1L_a/S_0)_{CI}$, which is the actual funnel controlling the decay. The increase of the barrier in polar solvents, and thus the loss of the efficiency in the IC to the ground state, correlates with the relative difference of polarity of the ^1L_a state at its minimum, with a computed dipole moment of 5.54 D, and at the $(^1L_a/S_0)_{CI}$ structure, 1.20 D. The barrier to access the CI will be larger in polar solvents, due to the stabilization of the ^1L_a minimum with respect to the CI. The theoretical prediction can be compared with the experiment: the AMN fluorescence maxima originated at the ^1L_a minimum varies from 3.29 (hexane) to 2.96 eV (acetonitrile),[11] pointing to a stabilization of the $(^1L_a)_{min}$ minimum when the solvent polarity is increased.

The influence of a purely nπ^* charge-transfer state from a twisted amino conformation on the AMN photophysics was investigated by optimizing the lowest $^1A''$ root of C_s symmetry with a perpendicular NH_2 group, in which the nπ^* nature of the state is in that way forced by the symmetry. The state energy at the FC, with an origin band computed at 4.39 eV, is too high to participate in the low-energy photophysics of the system. Regarding the triplet states, the isc quantum yield has been established to decrease with the solvent polarity, from 0.40 in hexane to 0.10 in acetonitrile.[11] As shown in Tables 2 and 3 the T_2 $\pi\pi^*$ state lies close to the singlet $\pi\pi^*$ states and, despite the extremely low spin−orbit coupling elements that we have computed in all cases (<1 cm^{-1}), it could be expected that different isc processes $^1L_b-T_2$ and $^1L_a-T_2$ take place in various regions of the PEHs, in particular, close to the minimum of ^1L_a, where the T_2 state lies higher in energy than ^1L_a, suggesting a near singlet−triplet crossing. Furthermore, the energy is trapped for a long time at the minimum and the probability of transfer it to the T_2 (^3L_b) state (∼0.1 eV) is higher. The lowest-energy triplet T_1 state is populated from T_2 via an accessible CI. The T_1 state lies adiabatically at 2.35 eV with a dipole moment of 1.33 D (see Table 2) and an associated radiative lifetime of 0.1 ms. Taking into account the computed low dipole moments of the triplet states, in polar solvents the singlet−triplet energy gap with the much more polar ^1L_a state will increase, explaining the smaller isc rate in polar media.

5. Summary and Conclusions

The photophysics of AMN has been investigated by combining experimental time-resolved transient ionization measurements with femtosecond resolution and quantum-chemical ab initio CASPT2//CASSCF theoretical calculations. The two lowest electronic excited state ^1L_b and ^1L_a of $\pi\pi^*$ character are computed to lie very close in energy, with minima at 3.50 and 3.69 eV, respectively. The bright ^1L_a $\pi\pi^*$ state is essentially populated following excitation in the 330−267 nm studied region. Despite the theoretical calculations predict a surface crossing between ^1L_a and ^1L_b states, no signature of it is observed in the time-dependent measurements. According to the experiments, the system fundamentally remains on the ^1L_a state after going through the crossing region, this state being responsible of the anomalous emission observed in the fluorescence spectrum. The decay lifetime observed in the transients, τ_2, shortens from nanoseconds to 13.5 ps with the excitation energy in the 330−267 nm range. This lifetime is assigned at the low-energy part of the excitation range to the simultaneous relaxation of ^1L_a state by IC and isc. The IC is mediated by the CI $(^1L_a/S_0)_{CI}$ placed 0.7 eV above the minimum, which exhibits an ethene-like CI character, i.e., a ring deformation by twisting of the C=C double-bond neighbor of the amino group. The excitation energy excess above the location of the CI decreases the excited-state lifetime from nanoseconds to picoseconds and, hence, the fluorescence quantum yield. The photophysics of the system in solution, with a internal conversion process less efficient in polar phases, is explained on the sole basis of the difference between the highly polar ^1L_a state minimum, with a partial charge-transfer character from the coplanar amino group and the less polar ground state at the $(^1L_a/S_0)_{CI}$ conformation. In polar solvents the barrier to access the CI from the ^1L_a minimum largely increases due to the relative stabilization of the latter. A similar effect is expected for the singlet−triplet gaps, in particular at the ^1L_a state minimum, where the isc between the close-lying ^1L_a and T_2 states is more probable because of the longer lifetime of the singlet state at the minimum structure.

Acknowledgment. R.M., A.L., A.P.C., C.R., and F.C acknowledge the financial support of Spanish MICINN through Grant CTQ-2008-03234 and Consolider Program "Science and Applications of Ultrafast Ultraintense Lasers" CSD2007-00013. They also thank the Basque Government (BG) funding through a Complementary Action and UPV−EHU Consolidated Group Program. The experimental work was carried out at the Laser Facility of the SGIker UPV/EHU. The research has been also supported by projects CTQ2007-61260 and CSD2007-0010 Consolider-Ingenio in Molecular Nanoscience of the Spanish MEC/FEDER.

References and Notes

(1) Platt, J. R. *J. Chem. Phys.* **1949**, *17*, 484.
(2) Rubio, M.; Merchán, M.; Ortí, E.; Roos, B. O. *Chem. Phys.* **1994**, *179*, 395.
(3) Suzuki, K.; Demeter, A.; Kühnle, W.; Tauer, E.; Zachariasse, K. A.; Tobita, S.; Shizuka, H. *Phys. Chem. Chem. Phys.* **2000**, *2*, 981–991.
(4) Meech, S. R.; O'Connor, D. V.; Phillips, D.; Lee, A. G. *J. Chem. Soc., Faraday Trans. 2* **1983**, *79*, 1563.
(5) Beck, S. M.; Hopkins, J. B.; Powers, D. E.; Smalley, R. E. *J. Chem. Phys.* **1981**, *74*, 43.
(6) Behlen, F. M.; Rice, S. A. *J. Chem. Phys.* **1981**, *75*, 5672.
(7) Stockburger, S.; Gattermann, H.; Klusmann, W. *J. Chem. Phys.* **1975**, *63*, 4519.
(8) Montero, R.; Longarte, A.; Martínez, R.; Sánchez Rayo, M. N.; Castaño, F. *Chem. Phys. Lett.* **2009**, *468*, 134.
(9) Berden, G.; Meerts, W. L.; Plusquellic, D. F.; Fujita, I.; Pratt, D. W. *J. Chem. Phys.* **1996**, *104*, 3935.
(10) Jiang, S.; Levy, D. H. *J. Phys. Chem. A* **2002**, *106*, 8590.
(11) Rückert, I.; Demeter, A.; Morawski, O.; Kühnle, W.; Tauer, E.; Zachariasse, K. A. *J. Phys. Chem. A* **1999**, *103*, 1958.
(12) Fuss, W.; Pushpa, K. K.; Rettig, W.; Schmid, W. E.; Trushin, S. A. *Photochem. Photobiol. Sci.* **2002**, *1*, 255.
(13) Andersson, K.; Malmqvist, P. Å.; Roos, B. O. *J. Chem. Phys.* **1992**, *96*, 1218.
(14) Hertel, I. V.; Radloff, W. *Rep. Prog. Phys.* **2006**, *69*, 1897.
(15) Pedersen, S.; Zewail, A. H. *Mol. Phys.* **1996**, *89*, 1455.
(16) De Vico, L.; Olivucci, M.; Lindh, R. *J. Chem. Theory Comput.* **2005**, *1*, 1029.
(17) Serrano-Andrés, L.; Merchán, M.; Nebot-Gil, I.; Lindh, R.; Roos, B. O. *J. Chem. Phys.* **1993**, *98*, 3151.
(18) Roos, B. O.; Andersson, K.; Fülscher, M. P.; Malmqvist, P.-Å.; Serrano-Andrés, L.; Pierloot, K.; Merchán, M. *Adv. Chem. Phys.* **1996**, *93*, 219.
(19) Merchán, M.; Serrano-Andrés, L. In *Computational Photochemistry*; Olivucci, M., Ed.; Elsevier: Amsterdam, The Netherlands, 2005.
(20) Borin, A. C.; Serrano-Andrés, L. *Chem. Phys.* **2000**, *262*, 253.
(21) Serrano-Andrés, L.; Merchán, M. In *Encyclopedia of Computational Chemistry*; Schleyer, P. v. R., Schreiner, P. R., Schaefer, H. F., III, Jorgensen, W. L., Thiel, W., Glen, R. C., Eds.; Wiley: Chichester, U.K., 2004.
(22) Serrano-Andrés, L.; Merchán, M. *J. Mol. Struct. (THEOCHEM)* **2005**, *729*, 109.

(23) Olaso-González, G.; Merchán, M.; Serrano-Andrés, L. *J. Phys. Chem. B* **2006**, *110*, 24734.
(24) Serrano-Andrés, L.; Merchán, M.; Borin, A. C. *Proc. Natl. Acad. Sci. U.S.A.* **2006**, *103*, 8691.
(25) Serrano-Andrés, L.; Merchán, M.; Borin, A. C. *Chem.—Eur. J.* **2006**, *12*, 6559.
(26) Serrano-Andres, L.; Merchan, M.; Lindh, R. *J. Chem. Phys.* **2005**, *122*, 104107.
(27) Andersson, K.; et al. *MOLCAS*, version 6.4; Department of Theoretical Chemistry, Chemical Centre, University of Lund: Lund, Sweden, 2006.
(28) Karlström, G.; Lindh, R.; Malmqvist, P.-Å.; Roos, B. O.; Ryde, U.; Veryazov, V.; Widmark, P.-O.; Cossi, M.; Schimmelpfennig, B.; Neograd y, P.; Seijo, L. *Comput. Mater. Sci.* **2003**, *28*, 222.
(29) Veryazov, V.; Widmark, P.-O.; Serrano-Andrés, L.; Lindh, R.; Roos, B. O. *Int. J. Quantum Chem.* **2004**, *100*, 626.
(30) Strickler, S. J.; Berg, R. A. *J. Chem. Phys.* **1962**, *37*, 814.
(31) Rubio-Pons, O.; Serrano-Andrés, L.; Merchán, M. *J. Phys. Chem. A* **2001**, *105*, 9664.
(32) Lahmani, F.; Zehnacker-Rentien, A.; Coudert, L. H.; Zachariasse, K. A. *J. Phys. Chem. A* **2003**, *107*, 7364.
(33) Dufraisse, C.; Etienne, A.; Rutimeyer, B. *C. R. Acad. Sci.* **1953**, *237*, 1601.
(34) Trushin, S. A.; Fue, W.; Schmid, W. E. *J. Phys. B: At., Mol. Opt. Phys.* **2004**, *37*, 3987.
(35) Baskin, J. S.; Zewail, A. H. *J. Phys. Chem.* **1994**, *98*, 3337.
(36) Souto, M. A.; Michl, J. *J. Am. Chem. Soc.* **1978**, *100*, 6853.
(37) Majewski, W. A.; Meerts, W. L. *J. Mol. Spectrosc.* **1984**, *104*, 271.
(38) Johnson, J. R.; Jordan, K. D.; Plusquellic, D. F.; Pratt, D. W. *J. Chem. Phys.* **1990**, *93*, 2258.
(39) Böhm, M.; Tatchen, J.; Krugler, D.; Kleinermanns, K.; Nix, M. G. D.; LeGreve, T. A.; Zwier, T. S.; Schmitt, M. *J. Phys. Chem. A* **2009**, *113*, 2458.
(40) Merchán, M.; González-Luque, R.; Climent, T.; Serrano-Andrés, L.; Rodríguez, E.; Reguero, M.; Peláez, D. *J. Phys. Chem. B* **2006**, *110*, 26471.
(41) Serrano-Andrés, L.; Merchán, M.; Borin, A. C. *J. Am. Chem. Soc.* **2008**, *130*, 2473.
(42) Serrano-Andrés, L.; Merchán, M. In *Photostability and Photoreactivity in Biomolecules: Quantum Chemistry of Nucleic Acid Base Monomers and Dimers*. Leszczynski, J., Shukla, M., Eds.; Springer: The Netherlands, 2008.
(43) Wassam, W. A.; Lim, E. C. *J. Chem. Phys.* **1978**, *68*, 433.
(44) Mulder, W. H.; Párkányi, C. *J. Phys. Chem. A* **2002**, *106*, 11932.
(45) Serrano-Andrés, L.; Roos, B. O. *J. Am. Chem. Soc.* **1996**, *118*, 185.

JP9058752